Processing and Application of Ceramics 13 [2] (2019) 164–172
https://doi.org/10.2298/PAC1902164N

Structural, microstructural, dielectric and ferroelectric properties of $BaTiO_3$-based ceramics

Rashmi Rekha Negi, Mallam Chandrasekhar, Pavan Kumar*

Department of Physics and Astronomy, National Institute of Technology, Rourkela 769008, Odisha, India

Received 23 August 2018; Received in revised form 14 January 2019; Received in revised form 7 April 2019; Accepted 16 May 2019

Abstract

(1-x)$BaTiO_3$–x$CaCu_3Ti_4O_{12}$ ceramic powders (where x = 0, 0.02, 0.04, 0.06, 0.08 and 1) were synthesized by solid state reaction method and sintered at up to 1250 °C. Phase formation, elemental composition and microstructure of all the samples were investigated by XRD, EDX and FESEM, respectively. The BT-CCTO ceramic samples corresponding to x = 0.04 content showed the best dielectric properties. The improvement of dielectric properties was attributed to the presence of oxygen vacancies. Ferroelectricity was retained for CCTO content up to x = 0.06.

Keywords: *structure, microstructure, dielectric, ferroelectric, non-ferroelectric*

I. Introduction

High dielectric constant materials are widely used in microelectronic devices due to small capacitive components which provide the opportunity of size reduction of the electronic devices [1,2]. Barium titanate ($BaTiO_3$, BT) based perovskite ferroelectrics possess high dielectric constant (ε_r) and low dielectric loss ($\tan\delta$) [3]. However, they possess a maximum value of ε_r at transition temperature (T_C), which is above the room temperature (RT), and the sharp phase transition at T_C has high temperature sensitive dielectric properties. Also, successive phase transitions of this system make the dielectric properties temperature dependent, which is not suitable from device application point of view [4–6]. Temperature stability of the dielectric properties of BT system can be enhanced by preparing its solid solutions with other compounds having temperature independent dielectric properties [4]. The crystal structure, microstructure and dielectric properties of BT ceramics can also be improved by doping with small concentrations [7,8].

Calcium copper titanate ($CaCu_3Ti_4O_{12}$, CCTO) is a non-ferroelectric perovskite type material, possessing a gigantic value of ε_r at RT. This system shows the high value of $\varepsilon_r \sim 10^4$–10^5, which is independent of frequency (10^2–10^6 Hz) and is almost constant in the 100–600 K temperature range [9–12]. CCTO ceramics neither exhibit any phase transition nor a crystal structure change in the temperature range of 35–1273 K [6]. The high dielectric constant of CCTO system is accounted in terms of extrinsic effects. The widely accepted mechanism for high ε_r in non-ferroelectric ceramics is an internal barrier layer capacitance (IBLC) model. In this model, the giant dielectric response is associated with the grain-boundary IBLC effect in the CCTO system [13,14]. The IBLC model is applicable to the ceramics which shows electrical microstructural heterogeneity, where the grain boundaries are highly resistive, much more than the grains, giving rise to high capacitance and thus the giant permittivity of the system [15,16]. In spite of seemingly important possible applications of these high ε_r non-ferroelectric materials, $\tan\delta$ of these materials is too high, which hinders the use of these materials in practical application [17]. Therefore, materials with high ε_r, low $\tan\delta$ and good temperature and frequency stability over a wide range are highly desired to be used in multilayer capacitor applications. With the incorporation of CCTO into the BT system, we expect an improvement in the dielectric properties along with the retention of ferroelectric properties.

In the present work, (1-*x*)BT–*x*CCTO samples are synthesized by solid state reaction route. Structural, surface morphological, dielectric and ferroelectric proper-

*Corresponding author: tel: + 91 661-2462726,
e-mail: *pvn77@rediffmail.com*

ties were analysed by XRD, FESEM, EDX, dielectric spectroscopy and ferroelectric measurements.

II. Experimental

$BaTiO_3$-based ceramic powders with different amount of $CaCu_3Ti_4O_{12}$ ($(1-x)BaTiO_3$–$xCaCu_3Ti_4O_{12}$, BT-CCTO, where x = 0, 0.02, 0.04, 0.06 and 0.08) were prepared by solid state reaction method. For comparison, the pure $CaCu_3Ti_4O_{12}$ powder was also prepared by the same method. $BaCO_3$ (CDH with > 99% purity), TiO_2 (MERCK with ≥ 98.5% purity), $CaCO_3$ (MERCK with ≥ 98.5% purity) and CuO (SD's with ≥ 97% purity) are used as the starting precursors. The stoichiometric amounts of the precursors were taken in polyethylene container along with zirconia balls and acetone as the grinding medium and were ball milled for 16 h. The milled BT and BT-CCTO powders were then dried and calcined at 1100 °C for 4 h with a slow heating rate of 5 °C/min in air atmosphere, and only the pure CCTO powder was calcined at 1050 °C for 4 h. The calcined powders were then mixed with polyvinyl alcohol (3 wt.%) as binder, ground and pressed by hydraulic press to form pellets of ~1 cm diameter and ~0.1 cm thickness. The BT pellets were sintered at 1250 °C for 4 h, and the pellets of the pure CCTO were sintered at 1100 °C for 8 h, with a slow heating rate of 5 °C/min in air atmosphere. The BT-CCTO pellets with x = 0.02 were sintered at 1250 °C for 4 h, whereas the BT-CCTO pellets having x = 0.04 to 0.08 were sintered at 1150 °C for 4 h, with a slow heating rate of 5 °C/min in air atmosphere.

X-ray diffraction (XRD) technique (Rigaku Ultima IV X-ray diffractometer, Tokyo, Japan) was used to identify the purity of phase of the calcined powders and sintered pellets. XRD patterns were obtained by Cu Kα source with 2θ ranging from 20° to 80° and a scanning rate of 6 °/min, The experimental density of the sintered pellets was measured by the Archimedes principle, using kerosene oil as an immersion liquid. For micrograph images, the sintered pellets were coated with Au electrode and the images were obtained using a field emission scanning electron microscope (FE-SEM, NOVA nano SEM). For electrical measurements, silver paste was deposited on both flat surfaces of the sintered pellets and fired at 400 °C for 30 min for good electrical contact. Dielectric parameters such as ε_r and $\tan\delta$ as a function of frequency and temperature were measured by using a precision LCR meter (HIOKI3532-50 LCR-HITESTER). RT polarization vs. electric field (P-E) loops were obtained by using Radiant precision premier II.

III. Results and discussion

3.1. Structure

Figure 1a shows the XRD pattern of the calcined samples. The results confirm the single-phase formation in the pure BT (x = 0) and CCTO (x = 1) ceramic powders. XRD pattern of the BT-CCTO calcined powder with x = 0.02 shows the presence of BT phase peaks only. However, with the increase in x fraction, CuO phase is observed for the ceramic sample with 4 mol% of CCTO (x = 0.04). With the further increase in x fraction, XRD peaks of CuO along with CCTO and an impurity phase (IP) are observed.

Figure 1b shows the XRD pattern of the sintered ceramics. XRD patterns of the pure BT (x = 0) and CCTO (x = 1) ceramic samples have sharp and well-defined single-phase peaks having tetragonal and cubic structure, respectively. There is a splitting of XRD peak at 2θ ~ 45° of the BT ceramics, which confirms the tetragonal structure of BT [18]. The BT-CCTO ceramic samples with x = 0.04, 0.06 and 0.08 show the presence of a major BT phase with minor secondary phase peaks of CuO. The presence of minor secondary phase XRD peaks can be explained with the fact that decomposition of CCTO ceramics occurs at high processing temperatures [6,13]. Whereas, the BT-CCTO ceramic samples with x = 0.02 have BT single-phase structure, which could indicate on the formation of solid solution with BT system. The ionic radius of Ca^{2+} is 1.34 Å and that of Ba^{2+} is 1.61 Å. Due to the smaller ionic radii of Ca^{2+} ions in comparison to larger Ba^{2+} ions, Ca^{2+} ions can occupy Ba^{2+} ions site in BT lattice. The ionic radius of

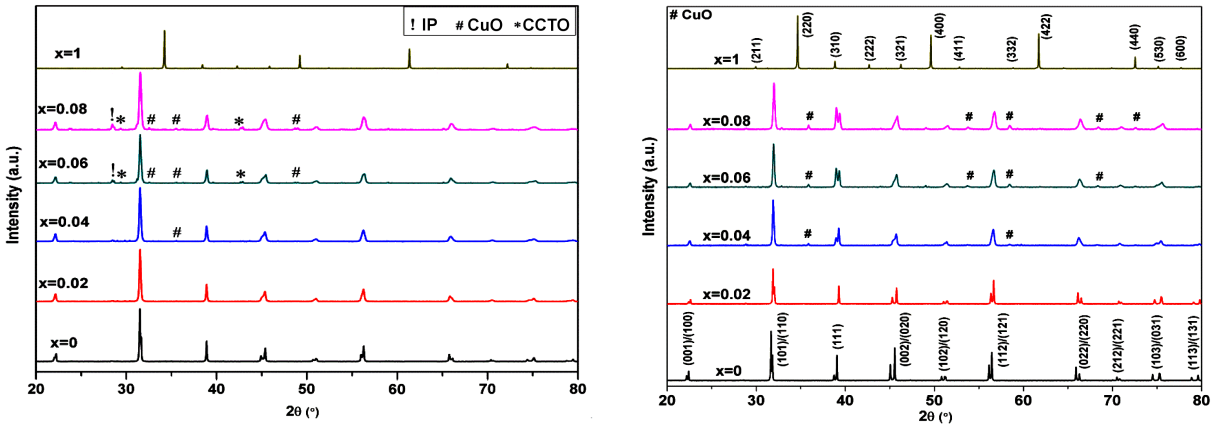

Figure 1. XRD patterns of: a) calcined and b) sintered BT-CCTO samples

Cu^{2+} is 0.73 Å, which is very close to the ionic radius of Ti^{4+} ions. Therefore, Cu^{2+} ions can occupy Ti^{4+} site in BT lattice [19]. There is also a peak splitting observed at $2\theta \sim 40°$ for the BT-CCTO ceramic samples with $x = 0.04$ to 0.08. This is due to the presence of CuO phase (matched with JCPDS No: 74-1021) at the same peak position as that of BT phase peaks (matched with JCPDS No: 75-1169), which merges and thus causes peak splitting. However, there is no peak splitting observed for $x = 0.02$ ceramic samples because of the absence of any CuO phase.

Experimental density (d_{exp}) of the sintered ceramic samples were calculated by using Archimedes formula [20]:

$$d_{exp} = \frac{w_{dry}}{w_{dry} - w_{sus}} d_k \quad (1)$$

where, w_{dry} and w_{sus} are the dry and suspended weights of the ceramic samples and $d_k = 0.81$ g/cm^3 is the density of kerosene oil, respectively. The densities of the sintered BT-CCTO ceramics have general trend to decrease with the increase of CCTO content (Table 1). However, only the sample having $x = 0.04$ shows different behaviour. Here, density of the prepared ceramic samples is associated with two factors: i) occupancy of Ba^{2+} ions site by Ca^{2+} ions which results in decrease of density [21] and ii) presence of CuO grains in BT system which results in increase of density [13]. The highest density (similar with that of the pure BT) of the BT-CCTO with $x = 0.04$ indicated on the already mentioned structural changes related to formation of secondary phase. Thus, the complementary cancellation of occupancy of Ba^{2+} by Ca^{2+} ions and segregation of CuO grains on the grain boundary could have the observed effect on density in the BT-CCTO system [13].

Figure 2 shows the FESEM micrographs of the sintered ceramic samples. Dense microstructures are observed in all the ceramic samples. The pure BT ceramics ($x = 0$) has large polyhedral grains, whereas the pure CCTO ceramics ($x = 1$) has polyhedral grains with signs of melted phase present at the grain boundaries. The melted phase at grain boundaries is found to be rich in CuO, as confirmed by EDX study (Fig. 3a). The BT-CCTO ceramic samples with $x = 0.02$ has uniform microstructure consisting of single-phase grains. However, the sintered ceramics with higher CCTO content (i.e. $x = 0.04$, 0.06 and 0.08) show a bimodal grain size distribution, one with larger elongated grains of few micrometers (1.90 to 2.02 μm) and other smaller polyhedral grains of hundreds of nanometers (250 to 290 nm). As confirmed from the EDX study (Fig. 3b), larger grains have the higher amount of Cu and O, and smaller grains contain more Ba, Ti, O along with Ca. This confirms the occupancy of Ca^{2+} ions at the Ba^{2+} site.

Table 1. Experimental density (d_{exp}) and average grain size (D) of (1-x)BT-xCCTO ceramics

Sample composition, x	d_{exp} [g/cm^3]	D [μm]
0	5.94	20.1
0.02	5.65	14.6
0.04	5.94	0.29
0.06	5.79	0.28
0.08	5.71	0.25
1	4.96	9.40

The average grain size was calculated by using the linear intercept method and the results are given in Table 1. The average grain size of BT ceramics decreases with increase in x content. However, a drastic decrease in the grain size is observed when the CCTO content increases from $x = 0.02$ to 0.04 and thereafter remains almost the same (for the ceramic samples with $x = 0.06$ and 0.08). The drastic decrease in average grain size of

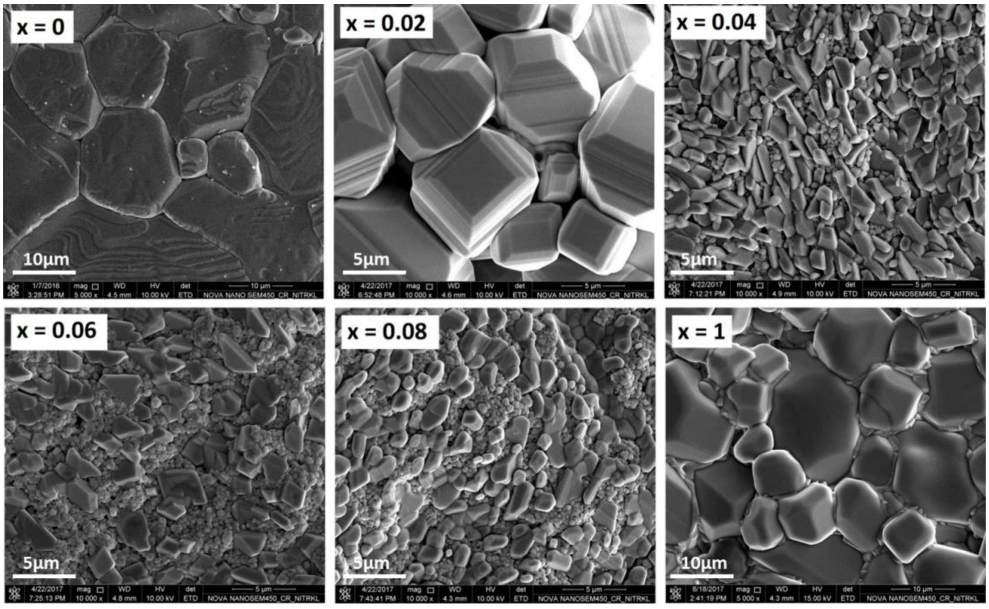

Figure 2. Surface micrographs of sintered BT-CCTO ceramics with different x fraction: a) 0, b) 0.02, c) 0.04, d) 0.06, e) 0.08 and f) 1

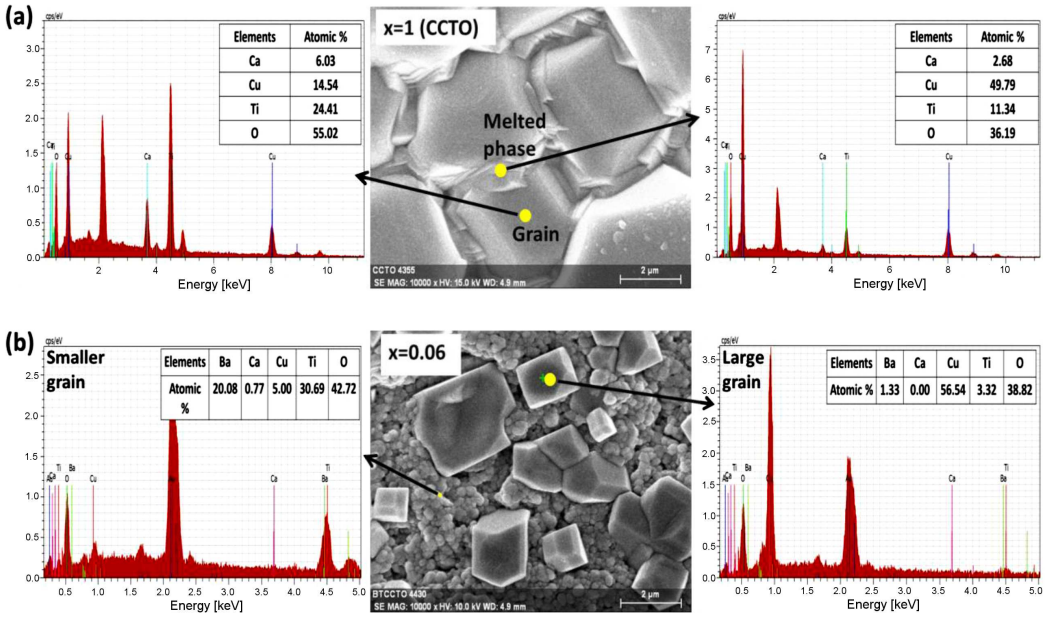

Figure 3. EDX data of: a) single grain and melted phase of the pure CCTO (x = 1) and b) large and small grains of the BT-CCTO ceramics having x = 0.06

BT from x = 0.02 to 0.04 ceramic samples is due to the presence of large elongated CuO grains, which inhibits grain growth of BT grains. However, from x = 0.04 to 0.08 ceramic samples, no significant variation in the grain sizes is observed. This indicates that both types of grains are present in the samples, which inhibits grain growth.

3.2. *Dielectric and ferroelectric properties*

Figure 4 shows the RT frequency dependence of ε_r and $\tan\delta$ of the sintered BT-CCTO ceramics and RT values of ε_r and $\tan\delta$ at 1 kHz are given in Table 2. Dielectric constant (ε_r) decreases with an increase of frequency for all the ceramic samples attributed to the decrease in net polarization of the ceramics [22]. Dielectric loss ($\tan\delta$) is high at low frequency and generally decreases with the increase of frequency for all the ceramic samples except for the pure CCTO (x = 1), where $\tan\delta$ is low at a lower frequency and increases with an increase of frequency. The higher $\tan\delta$ values at low and high frequency suggest the presence of dielectric relaxation process [23].

The high value of ε_r is observed for the CCTO system, which is attributed to the internal barrier layer capacitance (IBLC) mechanism [15]. This mechanism suggests the presence of electrical microstructure inhomogeneity in the ceramics, consisting of less resistive grains surrounded by high resistive grain boundaries. Thus, the grains serve as conducting plates and the grain boundaries serve as a dielectric material between the plates, together forming a number of parallel capacitors within the ceramics which increases the total capacitance thereby enhancing ε_r value [24]. From the microstructure and EDX studies of the pure CCTO, it is clear that the grain boundaries are rich in CuO phase which develop insulating layers in between the grains, and grains being more conducting than that of the grain boundary layers supports IBLC model.

Values of ε_r and $\tan\delta$ are found to increase with the increase of x content, but only for the sample BT-CCTO with x = 0.04 low $\tan\delta$ values are observed (Fig. 4). High value of $\tan\delta$ at low frequency of the BT-CCTO ceramics with x = 0.02 can be accounted in terms of increase in space charge polarization [25]. As can be seen from Fig. 1b, in the BT-CCTO ceramics with x = 0.02, XRD peaks corresponds to BT phase without any secondary phase. Moreover, the grain size of ceramic samples having x = 0.02 is higher than for other BT-CCTO ceramics. The absence of any secondary phase peaks and larger grain size of the BT-CCTO ceramics having x = 0.02 can facilitate large mobile charge accumulation at grain boundaries, thereby increasing space

Table 2. Dielectric and ferroelectric properties of (1-x)BT-xCCTO ceramics

Sample composition, x	ε_r (1 kHz & RT)	$\tan\delta$ (1 kHz & RT)	T_C (1 kHz)	γ [kV/cm]	E_c [μC/cm^2]	P_r
0	1136	0.06	149	1.05	4.86	6.73
0.02	1536	0.57	166	1.60	4.15	1.99
0.04	1582	0.07	170	1.62	3.21	1.28
0.06	1746	0.23	176	1.73	5.81	3.65
0.08	1788	0.49	200	-	-	-
1	1.9×10^4	0.14	-	-	-	-

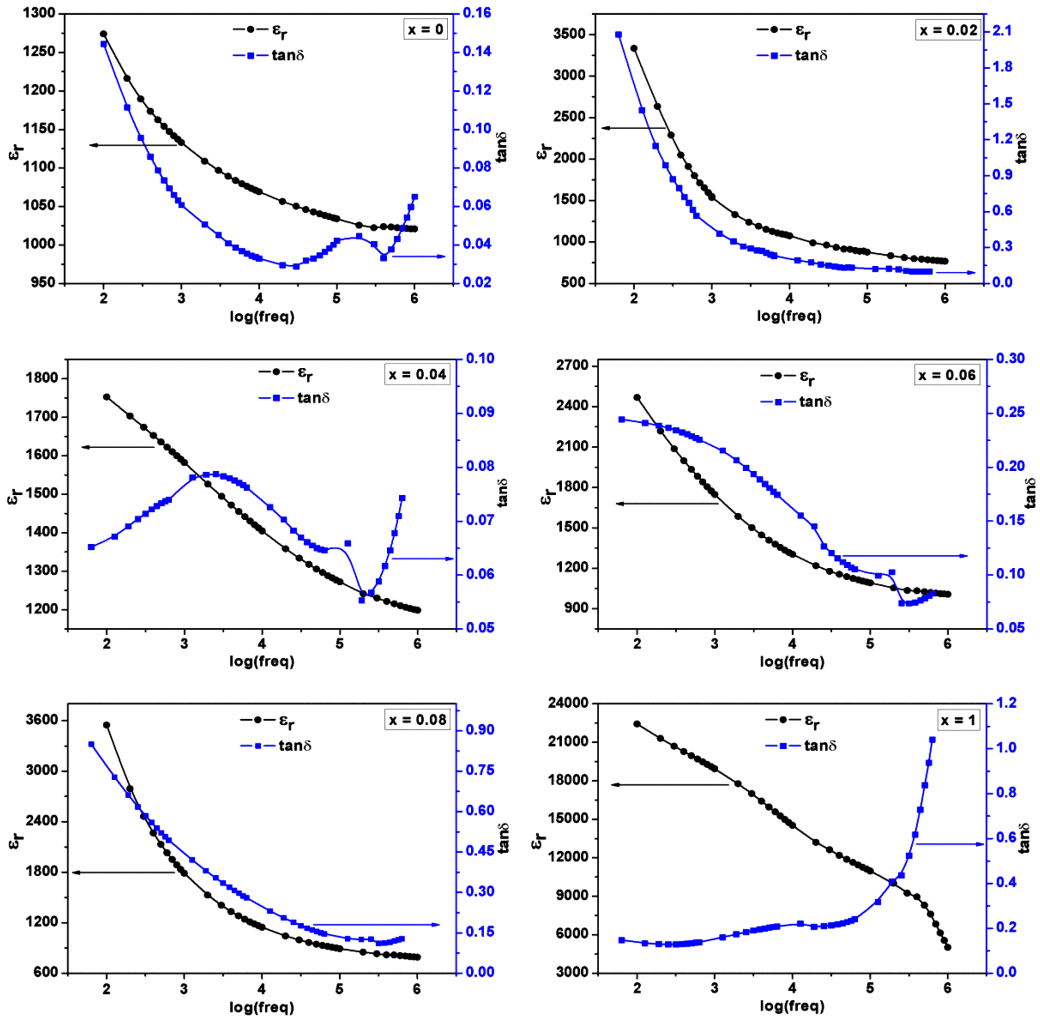

Figure 4. RT frequency dependence of ε_r of BT-CCTO ceramics with different x fraction: a) 0, b) 0.02, c) 0.04, d) 0.06, e) 0.08 and f) 1

charge polarization, which increases its tan δ value [26]. Increase in ε_r value with the increase of x content may be associated with the increase in amount of oxygen vacancies in the BT-CCTO samples [27]. Cu^{2+} (0.73 Å) ions have ionic radii close to Ti^{4+} (0.61 Å) ions, which can occupy Ti^{4+} ions site in $BaTiO_3$ lattice. However, Cu^{2+} has lower valence state compared to $Ti_4{}^+$, which can create negative charges in the doped BT system. In order to compensate these negative charges, oxygen vacancies are created [27]. Therefore, with the increase in x content, the amount of oxygen vacancies can be increased and thereby the dielectric constant of the BT-CCTO samples is increased [19,28]. Among all the BT-CCTO samples, the one with $x = 0.04$ shows best dielectric properties with high ε_r value and low loss which makes this system suitable for capacitor applications.

Figure 5 shows the temperature dependence of ε_r for the sintered ceramics at different frequencies over a temperature range of 30–200 °C. Dielectric constant of the pure CCTO ceramics (Fig. 5f) remains constant with an increase in temperature up to 200 °C for all the frequencies except at 1 kHz, where the ε_r value starts rising ~150 °C onwards. Whereas, for the pure BT and BT-CCTO ceramic samples, ε_r value continuously increases with the increase in temperature up to the transition temperature (T_C), thereafter it starts decreasing with the further increase in temperature. Increase in ε_r value up to T_C temperature is due to the increase in the space charge polarization and a decrease in ε_r value after T_C is due to the phase transition from ferroelectric to paraelectric phase [29]. T_C value of the sintered ceramic samples at 1 kHz is given in Table 2. T_C value of BT system is found to be ~149 °C. There is a shift in T_C towards higher temperatures with the increase of x from 0.02 to 0.08. This is due to the substitution of Ba^{2+} with Ca^{2+} ions at A site [30,31] and can be explained in terms of increase of the tolerance factor (t) given by the following equation:

$$t = \frac{R_A + R_O}{\sqrt{2}(R_B + R_O)} \tag{2}$$

where, R_A, R_B and R_O are the ionic radii of A and B site cations and oxygen anion, respectively. Thus, when Ca^{2+} ions with smaller ionic radii occupy Ba^{2+} ionic site in BT system, t value is found to increase and causes increase in T_C value of doped BT ceramics [32].

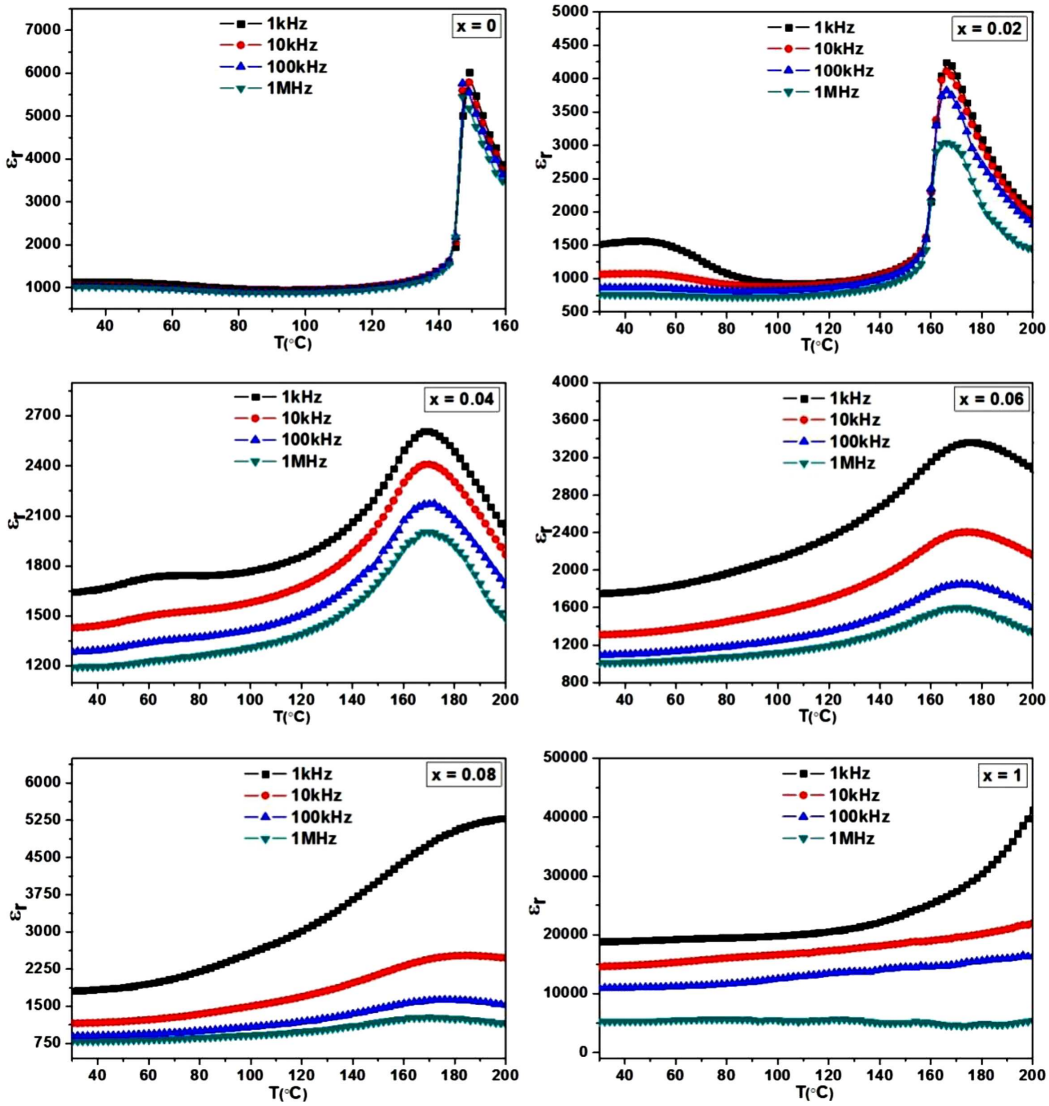

Figure 5. Temperature dependence of ε_r of BT-CCTO ceramics with different x fraction: a) 0, b) 0.02, c) 0.04, d) 0.06, e) 0.08 and f) 1

The pure BT system shows a sharp phase transition at T_C while the BT-CCTO ceramic samples show diffusive phase transition. The degree of diffusiveness in phase transition for the investigated ceramic samples is calculated by using the modified Curie-Weiss law, given by the following relation [33]:

$$\frac{1}{\varepsilon_r} - \frac{1}{\varepsilon_m} = \frac{(T - T_m)^\gamma}{C} \tag{3}$$

where, ε_r is the value of dielectric constant at temperature T, ε_m is the maximum value of dielectric constant at temperature $T = T_m$, C is the Curie constant and γ is the diffusivity factor which gives information regarding the behaviour of phase transition. The value of γ varies between 1 to 2, and if $\gamma = 1$ ceramics behaves as normal ferroelectrics while $\gamma = 2$ suggests its relaxor behaviour [34]. Figure 6 shows the variation of $\ln(1/\varepsilon_r - 1/\varepsilon_m)$ vs. $\ln(T - T_m)$ of the sintered ceramics at a frequency of 1 kHz. All the ceramic samples show linear behaviour and the value of γ is calculated by using a least square fitting method (Table 2). Value of γ increases with an increase in x content, indicating an increase in diffusiveness of the BT-CCTO ceramic samples. This diffusiveness suggests the occurrence of the intrinsic disorder by the replacement of the Ba^{2+} ions by the Ca^{2+} ions [30,35].

Figure 7 shows RT P-E hysteresis loops of the sintered ceramic samples. The presence of well saturated P-E hysteresis loop in the pure BT ($x = 0$) ceramics confirms its ferroelectric nature. However, saturation polarization decreases with the increase in x content and becomes lossy for the BT-CCTO with $x = 0.08$, thereby losing its ferroelectric nature [36]. P-E loops are characterized by the coercive field (E_c) and remnant polarization (P_r). These properties (Table 2) tend to decrease gradually with CCTO content up to $x = 0.04$, however their further increase for the BT-CCTO sample with $x = 0.06$ is obvious. Variation of E_c is in accordance with $\tan\delta$ value of the sintered ceramics. Thus, BT-CCTO

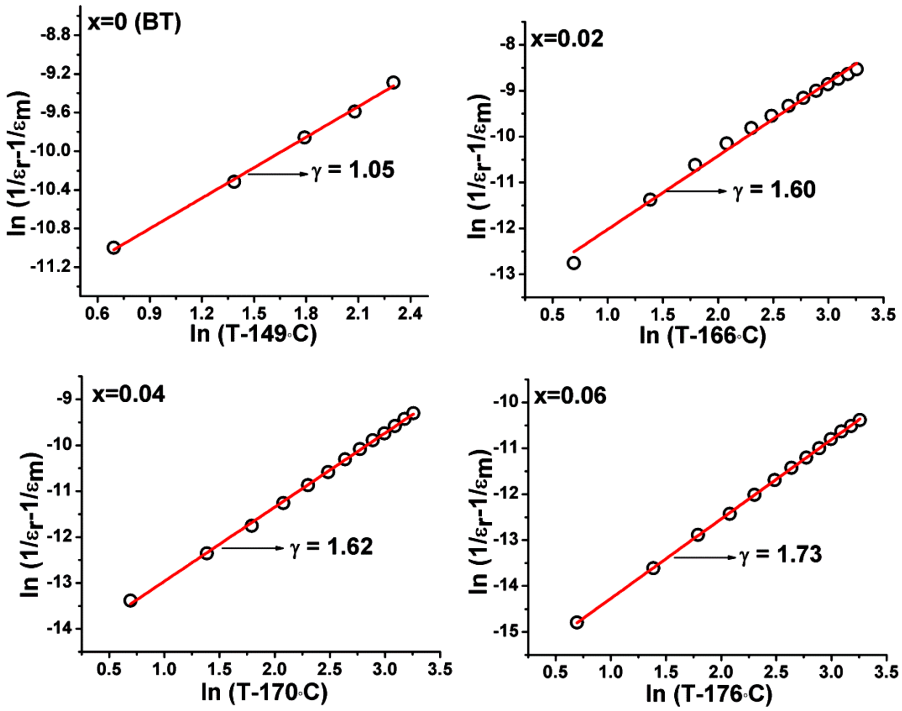

Figure 6. Variation of $\ln(1/\varepsilon_r - 1/\varepsilon_m)$ vs. $\ln(T - T_m)$ at 1 kHz of BT-CCTO ceramics with different x fraction: a) 0, b) 0.02, c) 0.04, d) 0.06, e) 0.08 and f) 1

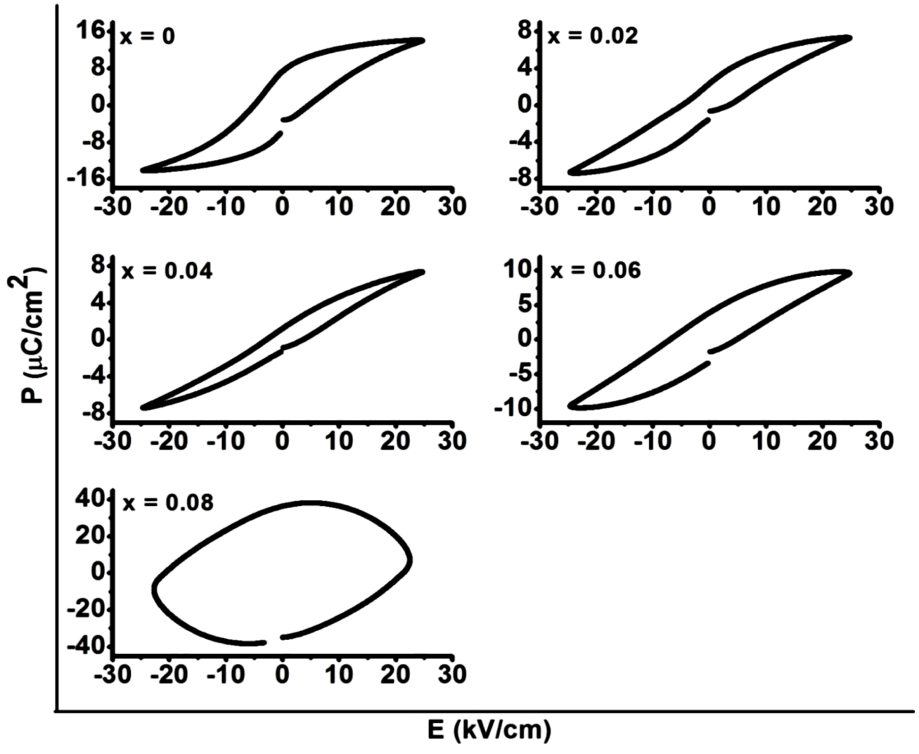

Figure 7. *P-E* hysteresis loops of BT-CCTO ceramics with different x fraction: a) 0, b) 0.02, c) 0.04, d) 0.06, e) 0.08 and f) 1

sample with $x = 0.04$ has the lowest E_c with the lowest dielectric loss. In addition, P_r value decreases with increase in x content from 0.02 to 0.04, which is related to the decrease in grain size of the ceramics [37]. The increase of x to 0.06 causes increase of P_r and it does not automatically mean the increase of ferroelectric nature of the samples. Thus, area of *P-E* loop increases due to increase in dielectric loss [38] and the sharpness of the loop decreases because of the increase in electrical conductivity [39]. Finally, for the BT-CCTO ceramics having $x = 0.08$ there is no saturation of *P-E* loop and it is characterised as a complete lossy material [36].

IV. Conclusions

(1-x)$BaTiO_3$–$xCaCu_3Ti_4O_{12}$ ceramic powders (where x = 0, 0.02, 0.04, 0.06 and 0.08) were prepared by solid state reaction method. For comparison, the pure $CaCu_3Ti_4O_{12}$ powder was also prepared by the same technique. The powders were uniaxially pressed and sintered at temperatures up to 1250 °C. Separately, single-phase formation in the pure BT (x = 0) and CCTO (x = 1) ceramic powders was confirmed from XRD study. The presence of secondary CuO phase (confirmed by XRD and EDX analyses) and bimodal grain size distribution (confirmed by FE-SEM analysis) were identified in the BT-CCTO ceramics having x = 0.04 to 0.08. Among all the BT-CCTO ceramics, the samples with x = 0.04 showed best dielectric properties at RT with dielectric constant of ~1582, low dielectric loss of ~0.07 at frequency of 1 kHz and diffusive phase transition with a high order of diffusivity (γ = 1.62) which makes this system suitable for capacitor applications. Transition temperature from ferroelectric to paraelectric phase increased with the increase of x content and among BT-CCTO ceramics the highest remnant polarization of $P_r \sim 3.65\,\mu C/cm^2$ was measured in the sample having x = 0.06.

References

1. T. Li, J. Chen, D. Liu, Z. Zhang, Z. Chen, Z. Li, X. Cao, B. Wang, "Effect of NiO-doping on the microstructure and the dielectric properties of $CaCu_3Ti_4O_{12}$ ceramics", *Ceram. Int.*, **40** (2014) 9061–9067.
2. L. Zhang, Z. Liu, G. Yang, X. Zhang, Z.Y. Cheng, "Nanoclip based composites with a low percolation threshold and high dielectric constant", *Nano Energy*, **26** (2016) 550–557.
3. K.M. Sangwan, N. Ahlawat, R.S. Kundu, S. Rani, S. Rani, N. Ahlawat, S. Murugavel, "Improved dielectric and ferroelectric properties of Mn doped barium zirconium titanate (BZT) ceramics for energy storage applications", *J. Phys. Chem. Solids*, **117** (2018) 158–166.
4. X. Chen, J. Chen, D. Ma, L. Fang, H. Zhou, "Thermally stable $BaTiO_3$-$Bi(Mg_{2/3}Nb_{1/3})O_3$ solid solution with high relative permittivity in a broad temperature usage range", *J. Am. Ceram. Soc.*, **98** (2015) 804–810.
5. Sonia, M. Chandrasekhar, P. Kumar, "Microwave sintered sol-gel derived $BaTiO_3$ and $Ba_{0.95}La_{0.05}TiO_3$ ceramic samples for capacitor applications", *Ceram. Int.*, **42** (2016) 10587–10592.
6. L. Singh, U.S. Rai, K.D. Mandal, B.C. Sin, H. Lee, H. Chung, Y. Lee, "Comparative dielectric studies of nanostructured $BaTiO_3$, $CaCu_3Ti_4O_{12}$ and $0.5\,BaTiO_3 \cdot 0.5\,CaCu_3Ti_4O_{12}$ nano-composites synthesized by modified sol-gel and solid state methods", *Mater. Charact.*, **96** (2014) 54–62.
7. V.S. Puli, D.K. Pradhan, B.C. Biggs, D.B. Chrisey, R.S Katiyar, "Investigations on structure, ferroelectric, piezoelectric and energy storage properties of barium calcium titanate (BCT) ceramics", *J. Alloys Compd.*, **584** (2014) 369S–373S.
8. M.M. Vijatović Petrović, J.D. Bobić, R. Grigalaitis, B.D. Stojanović, J. Banys, "La-doped and La/Mn-co-doped Barium Titanate Ceramics", *Acta Phys. Pol. A*, **124** (2013) 157–160.
9. M.A. Subramanian, D. Li, N. Duan, B.A. Reisner, A.W. Sleight, "High dielectric constant in $ACu_3Ti_4O_{12}$ and $ACu_3Ti_4O_{12}$ phases", *J. Solid State Chem.*, **151** (2000) 197–200.
10. A. Nautiyal, C. Autret, C. Honstettre, S.D. Almeida-Didry, M.E. Amrani, S. Roger, B. Negulescu, A. Ruyter, "Local analysis of the grain and grain boundary contributions to the bulk dielectric properties of $Ca(Cu_{3-y}Mg_y)Ti_4O_{12}$ ceramics: Importance of the potential barrier at the grain boundary", *J. Eur. Ceram. Soc.*, **36** (2016) 1391–1398.
11. L. Singh, U.S. Rai, K. Mandal, B.C. Sin, S. I. Lee, Y. Lee, "Dielectric, AC-impedance, modulus studies on $0.5\,BaTiO_3 \cdot 0.5\,CaCu_3Ti_4O_{12}$ nano-composite ceramic synthesized by one-pot, glycine-assisted nitrate-gel route", *Ceram. Int.*, **40** (2014) 10073–10083.
12. S. Rani, N. Ahlawat, R.S. Kunda, R. Punia, S. Kumar, K.M. Sangwan, N. Ahlawat, "Structural and dielectric properties of $Ca_{0.95}Nd_{0.05}Cu_3Ti_{3.95}Zr_{0.05}O_{12}$ ceramic", *Ferroelectrics*, **516** (2017) 156–166.
13. W. Yuan, "Investigation on the decomposable process and the secondary liquid phase effect on the dielectric properties of $CaCu_3Ti_4O_{12}$ ceramics", *J. Phys. D: Appl. Phys.*, **42** (2009) 175401.
14. B. Samanta, P. Kumar, C. Prakash, "Effect of sintering temperature and Cu-rich secondary phase on dielectric properties of microwave processed $CaCu_3Ti_4O_{12}$ ceramics", *Ferroelectrics*, **517** (2017) 46–57.
15. D.C. Sinclair, T.B. Adams, F.D. Morrison, A.R. West, "$CaCu_3Ti_4O_{12}$: One step internal barrier layer capacitor", *Appl. Phys. Lett.*, **80** (2002) 2153–2155.
16. A.R. West, T.B. Adams, F.D. Morrison, D.C. Sinclair, "Novel high capacitance materials: $BaTiO_3$:La and $CaCu_3Ti_4O_{12}$", *J. Eur. Ceram. Soc.*, **24** (2004) 1439–1448.
17. O.A.A. Abdelal, A.A. Hassan, M. El-Sayed Ali, "Dielectric properties of calcium copper titanates ($CaCu_3Ti_4O_{12}$) synthesized by solid state reaction", *Int. J. Sci. Res.*, **3** (2014) 1356–1361.
18. P. Sharma, P. Kumar, R.S. Kundu, J.K. Juneja, N. Ahlawat, R. Punia, "Structural and dielectric properties of substituted barium titanate ceramics for capacitor applications", *Ceram. Int.*, **41** (2015) 13425–13432.
19. R.D. Shannon, "Revised effective ionic radii and systematic studies of interatomic distances in halides and chalcogenides", *Acta Cryst. A*, **32** (1976) 751–767.
20. R.R. Negi, P. Kumar, "Comparative studies of BT, LCNO, 0.96BT-0.04LCNO ceramics for capacitor applications", *Ceram. Int.*, **44** (2018) 14311–14317.
21. Sonia, R.K. Patel, C. Prakash, P. Kumar, "Effect of microwave processing on structural, dielectric and ferroelectric properties of calcium-doped $BaTiO_3$ ceramics", *J. Ceram. Process. Res.*, **12** (2011) 634–639.
22. M. Chandrasekhar, P. Kumar, "Synthesis and characterizations of BNT-BT-KNN ceramics for energy storage applications", *Phase Transit.*, **89** (2016) 944–957.
23. M. Chandrasekhar, P. Kumar, "Synthesis and characterization of BNT-BT and BNT-BT-KNN ceramics for actuator and energy storage applications", *Ceram. Int.*, **41** (2015) 5574–5580.
24. B. Khumpaitol, J. Khemprasit, "Improvement in dielectric properties of Al_2O_3-doped $Li_{0.30}Cr_{0.02}Ni_{0.68}O$ ceramics", *Mater. Lett.*, **65** (2011) 1053–1056.

25. Ch. Rayssi, S. El. Kossi, J. Dhahri, K. Khirouni, "Frequency and temperature-dependence of dielectric permittivity and electric modulus studies of the solid solution $Ca_{0.85}Er_{0.1}Ti_{1-x}Co_{4x/3}O_3$ ($0 \leq x \leq 0.1$)", *RSC Adv.*, **8** (2018) 17139–17150.
26. K.C. Kao, *Dielectric Phenomena in Solids: With Emphasis on Physical Concepts of Electronic Processes*, Elsevier Academic Press, USA, 2004.
27. S.K. Kar, S. Swain, Sonia, P. Kumar, "High dielectric constant and low optical band gap studies of La-modified $Ba(Fe_{0.5}Nb_{0.5})O_3$ ceramics", *Mater. Chem. Phys.*, **155** (2015) 171–177.
28. H. Suna, Y. Zhang, X.F. Liu, Y. Liu, W. Chen, "Effects of CuO additive on structure and electrical properties of low-temperature sintered $Ba_{0.98}Ca_{0.02}Zr_{0.02}Ti_{0.98}O_3$ lead-free ceramics", *Ceram. Int.*, **41** (2015) 555–565.
29. P. Kumar, P. Singh, J.K. Juneja, K.K. Raina, R.P. Pant, C. Prakash, "Structural, dielectric and ferroelectric properties of PLZFNT ceramics", *J. Alloys Compd.*, **601** (2014) 207–211.
30. R. Varatharajan, S.B. Samanta, R. Jayavel, C. Subramanian, A.V. Narlikar, P. Ramasamy, "Ferroelectric characterization studies on barium calcium titanate single crystals", *Mater. Charact.*, **45** (2000) 89–93.
31. Y. Noguchi, M. Miyayama, T. Kudo, "Direct evidence of A-site-deficient strontium bismuth tantalite and its enhanced ferroelectric properties", *Phys. Rev. B*, **63** (2001) 214102-5.
32. H. Zou, X. Hui, X. Wang, D. Peng, J. Li, Y. Li, X. Yao, "Luminescent, dielectric, and ferroelectric properties of Pr doped $Bi_7Ti_4NbO_{21}$ multifunctional ceramics", *J. Appl. Phys.*, **114** (2013) 223103–223107.
33. S. Swain, P. Kumar, D.K. Agrawal, Sonia, "Dielectric and ferroelectric study of KNN modified NBT ceramics synthesized by microwave processing technique", *Ceram. Int.*, **39** (2013) 3205–3210.
34. S. Sharma, K. Sharma, A. Ranjan, R. Rai, P. Kumar, S. Sinha, "Impedance and modulus spectroscopy characterization of lead free barium titanate ferroelectric ceramics", *Ceram. Int.*, **41** (2015) 7713–7722.
35. V.S. Tiwari, D. Pandey, "The influence of a powder processing technique on chemical homogeneity and the diffuse phase transition behaviour of $Ba_{0.9}Ca_{0.1}TiO_3$ ceramics", *J. Phys. D: Appl. Phys.*, **22** (1989) 837–843.
36. B. Jaffe, W. Cook, H. Jaffe, *Piezoelectric Ceramics*, Academic Press, London, 1971.
37. X. Li, J. Wang, "Effect of grain size on the domain structures and electromechanical responses of ferroelectric polycrystal", *Smart Mater. Struct.*, **26** (2017) 015013–015026.
38. M. Stewart, M.G. Cain, D.A. Hall, "Ferroelectric hysteresis measurement and analysis", *Technical Report CMMT (A) 152*, National Physical Laboratory, Teddington, United Kingdom, 1999.
39. L.M. Levinson, *Electronic Ceramics: Properties, Devices, and Applications*, Marcel Dekker Inc., New York, 1988.